RSC Advances

ROYAL SOCIETY OF CHEMISTRY

www.rsc.org/advances

Journal Name

ARTICLE

A salification-induced charge transfer effect for improving the resistive memory performance of azo derivative-based devices

Received 00th January 20xx,
Accepted 00th January 20xx

DOI: 10.1039/x0xx00000x

www.rsc.org/

Quan Liu,[a] Qingfeng Xu,[a] Huilong Dong,[b] Hua Li,[a] Dongyun Chen,[a] Lihua Wang,[a] Youyong Li[b] and Jianmei Lu*[a]

In this study, we report the synthesis of a new organic conjugate molecule, 3-(4-((4-(dimethylamino)phenyl)diazenyl)phenyl)-1-(pyridin-4-yl)prop-2-en-1-one (**AZOCP**), and its camphorsulfonic acid salt (**AZOCP-CSA**). The photophysical and electrochemical characterization reveals that an enhanced π–π conjugation is formed in the camphorsulfonic acid salt because of the salification effect. The salification reaction also play an important role in the formation of a more ordered stacking nanocrystalline film as evidenced by AFM and XRD analysis, and thus gives rise to an improved transport of charge carriers. The comparison of device performance demonstrates that the device based on the use of the salificated compound has better resistive memory behaviour in terms of ON/OFF ratio, retention time and rewritable cycle. Isothermal I–V correction and theoretic calculation confirm that the resistive performance is a result of an electric-field-induced charge transfer effect and the enhanced device performance of camphorsulfonic acid salt is due to the presence of a strong salification-induced charge transfer effect. Our experimental finding suggests that the simple but effective salification strategy may find widespread use in promoting performance of other organic resistive memory devices by introducing a strong charge transfer effect.

Introduction

Since the resistive behavior was proposed, a great deal of research interest has been devoted to the development of various resistive materials for practical application.[1-4] The resistive memory is recognized as an appealing candidate for the next generation "universal memory" due to its high density, low power consumption, large ON/OFF ratio, high endurance and long retention.[5-10] Therefore, a variety of materials and strategies for memory application has been provided.[11, 12] Among them, organic small molecules based memories due to their tunable functionalization and easy device miniaturization are becoming the most promising materials to realize high-performance resistiveperformance.[13-16]

A variety of design approaches for organic molecule-based resistive memory devices have already been reported in the literature.[17-28] To tune the memory performance, one of the most common methods is blending with other salt or dyes. [29] for instance, Meskers once introduced a series of inorganic salt ($LiCF_3SO_3$ or NaCl) in the polymer layer results in resistive switching behavior under external electric field.[30,31] It has been suggested that the migration of the dopant ions into and out of the polymer depletion layer at the aluminum Schottky contact causes resistive bistability behavior. Our group previously reported facilely blending the donor and acceptor moieties of the D–π–A framework as the active materials for resistive switching memory, and the change of the blend ratio to tune electrical data storage performance from volatile to non-volatie.[32] However, the proportion of the blend part has great effect on the performance, and the inevitable separation of the blend phase will also have a great impact on the memory performance.

The method of salification not only can effectively promote the thermal stability of the compound,[33] but also can improve the

[a] College of Chemistry, Chemical Engineering and Materials Science, Key Laboratory of Adsorption Technology in Petroleum and Chemical Industry for Wastewater Treatments, Soochow University, 199 Ren'ai Road, Suzhou 215123, China
Fax: +86 512 65880367; Tel: +86 512 65880368; E-mail: lujm@suda.edu.cn,
[b] Functional Nano & Soft Materials Laboratory (FUNSOM) and Jiangsu Key Laboratory for Carbon-Based Functional Materials & Devices, Soochow University, Suzhou, 215123, China
Electronic Supplementary Information (ESI) available: [Spectral data, Figure S1-S4. Thermogravimetric analysis of the both molecules, Figure S5. Current–voltage (I–V) characteristics, the endurance cycles and the effect of retention time of **AZOCP2** and **AZOCP-CSA**, Figure S6.]. See DOI: 10.1039/x0xx00000x

uniformity and stability of the films.[34] Li *et al.* has designed and reported protonic-acid-doped poly(Schiff base) resistive memory devices, which has long consecutive switching cycles and excellent operative uniformity.[35] However, the application of salification to tune the memory performance of small molecules was seldom reported.

In this work, we synthesized a new conjugated molecule containing a pyridine as end group: 3-(4-((4-(dimethylamino)phenyl)diazenyl)phenyl)-1-(pyridin-4-yl)prop-2-en-1-one (**AZOCP**). Then, camphorsulfonic acid (**CSA**) was used as a salification agent to formed **AZOCP-CSA**.[36] The **AZOCP-CSA** can be effectively obtained by tuning the **AZOCP**/**CSA** ratio, which can be accurately confirmed by ^{1}H NMR spectroscopy (Figure S4). However, when increasing the amount of camphorsulfonic acid to change the **AZOCP**/**CSA** ratioto1/2, the compound can not avoid moisture absorption in the air and hard to forming a film. By contrast, **AZOCP-CSA** with ratio of 1/1 has good solubility, thermal stability and fine film-forming properties. Then, fabricated Au/**AZOCP**/ITO and Au/**AZOCP-CSA**/ITO devices and their resistance-switching parameters have been studied in details. Specifically, the Au/**AZOCP-CSA**/ITO device shows a greater performance improvement and a promising potential for information storage applications.

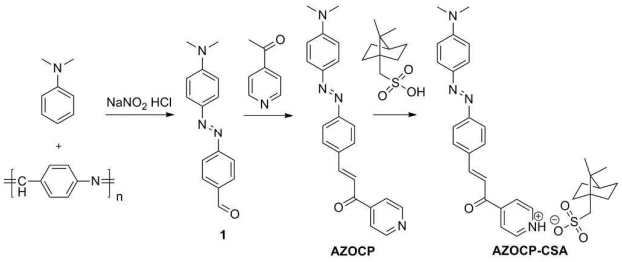

Scheme 1 The synthetic routes and molecular structures of **AZOCP** and **AZOCP-CSA**.

Experimental

Materials

Sodium nitrite, 4-aminobenzaldehyde polymer, anhydrous sodium acetate, N, N-dimethylaniline, 1-(pyridin-4-yl)ethanone, camphorsulfonic acid were purchased from commercial sources (TCI, Alfa Aesar, and Sigma-Aldrich). All solvents were purchased from Sinopharm Chemical Reagent Co., Ltd. All chemicals were used as received without further purification.

Characterization

All electrical measurements of the device were characterized under ambient conditions without any encapsulation using Keithley 4200 semiconductor characterization system in voltage sweeping mode. The sweeping step is 0.01 V. ^{1}H nuclear magnetic resonance (^{1}H NMR) spectra were measured at 400 MHz on a Bruker 400 AVANCE spectrometer with dimethyl sulfoxide-d_6 (DMSO-d_6) as the solvent. High-resolution mass spectra (HRMS) were acquired using a Micro mass GCT-TOF mass spectrometer with an electrospray ionization source. UV-Vis absorption spectra were recorded on a Shimadzu UV-3600 spectrophotometer at room temperature. Thermogravimetric analysis (TGA) was performed on a Perkin-Elmer Diamond TG/DTA instrument under a nitrogen atmosphere with the gas-flow rate of 50 mL/min and a heating rate of 10 °C/min. Cyclic voltammetry (CV) measurements were carried out under an argon atmosphere. The film coated on a ITO electrode (working electrode) was scanned at 1 mV/s in a 0.1 M solution of tetrabutylammonium hexafluorophosphate (n-Bu4NPF$_6$) in acetonitrile, with Ag/AgCl (3.8 M KCl) and a platinum as the reference and counter electrodes, respectively. The atomic force microscopy (AFM) measurements were performed using a MFP-3DTM (Digital Instruments/Asylum Research) AFM instrument in the tapping mode. X-ray diffraction (XRD) patterns were collected using an X'Pert-Pro MPD X-ray diffractometer.

Fabrication of Memory Devices

The ITO substrates were pre-cleaned with ethanol, acetone and isopropanol sequentially in an ultrasonic bath for 20 min. A 0.1 mL benzene solution of **AZOCP** or **AZOCP-CSA** was spin-coated onto the substrates at a spinning speed of 500 rpm for 10 s and then 2000 rpm for 30 s, followed by a vacuum-drying at 80 °C for 8 h. Before spin-coating, the solution was filtered through polytetrafluoroethylene (PTFE) membrane micro-filters with a pore size of 0.32 μm. The thickness of the films is about 90 nm as measured by spectroscopic ellipsometer (model M2000DI, Woollam). To construct the Au/**AZOCP** or **AZOCP-CSA**/ITO structures, Au top electrodes was thermally evaporated onto the film surface under 2 × 10^{-6} Torr through a shadow mask with thickness around 60 nm and area of 0.20 mm^2.

Synthetic procedures

Synthesis of 4-((4-(dimethylamino)phenyl)diazenyl)benzaldehyde (**1**)

The 4-((4-(dimethylamino)phenyl)diazenyl)benzaldehyde was synthesized according to the previous literature.[37]

A solution of sodium nitrite (4.35 g, 0.063 mol) in water (24 mL) was added dropwise to a mixture of 4-aminobenzaldehyde polymer (6.03 g, 0.06 mol), water (32 mL) and concentrated hydrochloric acid (20 mL) at 0-5 °C. The mixture was stirred at 0-5 °C for 30 min. A mixture of N, N-dimethylaniline (8.0 g, 0.066 mol), concentrated hydrochloric acid (10 mL) and water (30 mL) was added slowly to the diazonium salt solution at 0-5 °C. After 1 h, anhydrous sodium acetate (18 g, 0.22 mol) was added to the resulting mixture, which was then stirred at 0-5 °C for 24 h. The solution was filtered and the obtained crude product was recrystallized from ethanol to afford compound **1** as a brown powder (yield 75%).

^{1}H NMR (400 MHz, DMSO-d_6) d (ppm): 10.06 (s, 1H, CHO), 8.05 (d, J = 8.0 Hz, 2H, ArH), 7.93 (d, J = 8.0 Hz, 2H, ArH), 7.85 (d, J = 8.0 Hz, 2H, ArH), 6.86 (d, J = 8.0 Hz, 2H, ArH), 3.09 (s, 6H, 2CH$_3$). ^{13}C NMR (100 MHz, DMSO-d_6): d (ppm): 192.4, 155.9, 153.1, 142.8, 136.0, 130.7, 125.5, 122.3, 111.6, 39.8.

Synthesis of 3-(4-((4-(dimethylamino)phenyl)diazenyl)phenyl)-1-(pyridin-4-yl)propp-2-en-1-one (**AZOCP**)

A solution of 10% aqueous sodium hydroxide (20.0 mL) was slowly added dropwise via a self-equalizing addition funnel to a stirred solution of **1** (20.0 mmol) and 1-(pyridin-4-yl)ethanone (20.0 mmol) in approximately 40 mL of methanol with an ice-water bath. The reaction solution was allowed to stir at room temperature for approximately 10 h. The formed precipitate was collected by suction filtration. Recrystallization from the methanol solvent afforded the pure product (yield 70%).

^{1}H NMR (400 MHz, $CDCl_3$) d (ppm): 8.85 (d, J = 4.4 Hz, 2H, ArH), 7.92-7.86 (m, 5H, ArH),7.79 (d, J = 5.6 Hz, 2H, ArH), 7.76 (d, J = 8.4 Hz, 2H, ArH), 7.47 (d, J = 16 Hz, 1H, ArH), 6.77 (d, J = 9.2 Hz, 2H), 3.12 (s, 6H, $2CH_3$). ^{13}C NMR (100 MHz, $CDCl_3$): d (ppm): 189.2 (C=O), 154.3 (Ar-C), 152.4 (Ar-C), 150.3 (Ar-C), 145.8 (Ar-C), 144.1 (Ar-C), 143.3 (Ar-C), 134.3 (Ar-C), 129.2 (Ar-C), 125.0 (Ar-C), 122.4 (Ar-C), 121.1 (Ar-C), 120.7 (Ar-C), 111.4 (C=C), 39.8 ($2CH_3$). HRMS: calcd for $C_{22}H_{20}N_4O$ $[M + H]^+$ 357.1715, found 357.1667.

Preparation of **AZOCP-CSA**.

The protonation of **AZOCP** by camphorsulfonic acid (**CSA**) was performed in chloroform at room temperature. A **CSA**/chloroform solution was added to an **AZOCP** /chloroform solution with the **CSA** to **AZOCP** molar ratio of 1:1. The salification process continued for one day to ensure thorough reaction. Chloroform was then removed by rotary evaporation followed by vacuum distillation at 80 ^{o}C for one day. By comparing the ^{1}H NMR spectra of **AZOCP-CSA** in $CDCl_3$, the ratio of the integral of CH_3 in **AZOCP** and CH_3 in **CSA** is 1 : 1 which means **AZOCP** and **CSA** are salified sucessfully. (Figure S4).

Results and discussion

AZOCP and **AZOCP-CSA** can be obtained via the synthetic routes as shown in Scheme 1. The thermal stability of **AZOCP** and **AZOCP-CSA** were evaluated by TGA under a nitrogen atmosphere. As shown in the TGA curves (Figure S5), the thermal decomposition temperature (the 5% weight-lost temperature) of **AZOCP** was 194 ^{o}C and that of **AZOCP-CSA** was up to 213 ^{o}C. The good-thermal stability of **AZOCP-CSA** could better endure heat deterioration in the memory devices.[38,39]

Photophysical and electrochemical properties

In view of the **AZOCP** and **AZOCP-CSA** has good solubility in polar solvent. So we choose chlorobenzene as the solvent and used spin coated method to fabricate the film. Figure 2 shows the optical absorption spectra of **AZOCP** and **AZOCP-CSA** nanofilms on quartz substrates. The weak energy absorption bands at 300-350 nm can be attributed to the π→π* transition of the azobenzene chromophore and the strong absorption bands at approximately 400-500 nm can be attributed to the n→π* transition (charge transfer) of the azobenzene.[40, 41] The optical band gaps of the **AZOCP** and **AZOCP-CSA** molecules, estimated from the absorption edges of the films, are 2.22 and 2.01 eV, respectively. Compared with that of **AZOCP**, the onset optical absorbance of **AZOCP-CSA** exhibits a significant red-shift for 21 nm, which corresponds to a narrower energy band gap of the salification system. Therefore, salificating **AZOCP** with camphorsulfonic acid gives rise to a ground state charge transfer complex in **AZOCP-CSA**. Meanwhile, it also suggests that the **AZOCP-CSA** film forms an ordered stacking of the π-conjugation system, favouring an effective carriers migration.

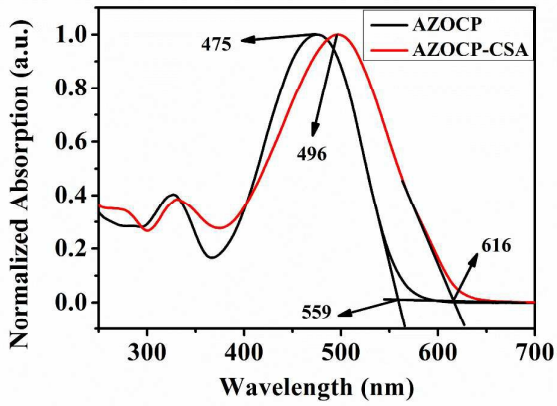

Figure 2 UV-vis spectra of the **AZOCP** and **AZOCP-CSA** thin films on quartz substrates.

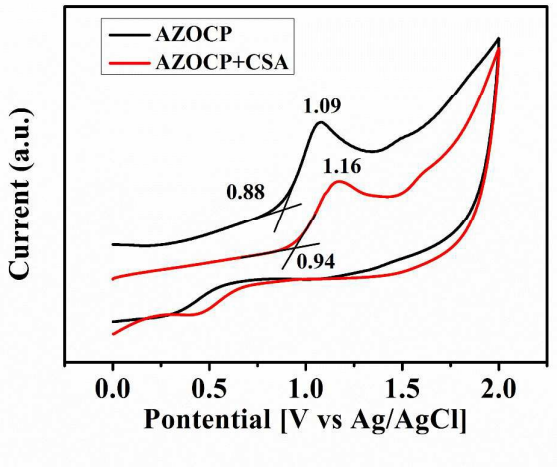

Figure 3 Cyclic voltammograms of **AZOCP** and **AZOCP-CSA** films on ITO substrates.

Figure 3 shows the cyclic voltammetry (CV) measurements of **AZOCP** and **AZOCP-CSA** on an indium-tin-oxide (ITO) glass substrate in a 0.1 mol L^{-1} solution of tetrabutylammonium hexafuorophosphate ($TBAPF_6$) in anhydrous acetonitrile solution; measurements were taken with a scan rate of 100 mV s^{-1}. The onset oxidation (E_{ox}^{onset}) of **AZOCP** and **AZOCP-CSA** are approximately 0.88 V and 0.94 V vs Ag/AgCl, respectively. The oxidation potential onset (E_{ox}^{onset}) of ferrocene was measured to be 0.44 V vs Ag/AgCl in acetonitrile with bare ITO glass. The estimated highest occupied molecular orbital (HOMO) levels can be calculated from the oxidation potential onset E_{ox}^{onset} according to the following formula: HOMO = -[E_{ox}^{onset} + 4.8-E_{Fc}] eV. The lowest unoccupied molecular orbital (LUMO) levels are not detectable from CV; the values of the LUMO levels were estimated from following formula: LUMO = [HOMO +E_g] eV. The HOMO levels of **AZOCP** and **AZOCP-CSA** are -5.24 eV and -5.3 eV, respectively. The determined LUMO levels of **AZOCP** and **AZOCP-CSA** are -3.02 eV and -3.17 eV, respectively (see Table S1). **AZOCP-CSA** has lower LUMO levels than **AZOC**P, which due to the charge transfer process, agreement with UV spectroscopic data.

Morphology of the thin film

To investigate the surface morphology and film microstructure, atomic force microscopy (AFM) and X-ray diffraction (XRD) measurements were carried out on the **AZOCP** and **AZOCP-CSA** films. As seen from the AFM height images (Figure 4), both of molecule films showed a relatively smooth surface without obvious defects. The **AZOCP** film clearly showed two-dimensional grains in its solid state at room temperature with uniform size and the surface root-mean-square (RMS) roughness is 4.45 nm. The **AZOCP-CSA** film showed a denser needle morphology, and a RMS roughness of 2.5 nm, smaller than that of **AZOCP**. Therefore, salification improves the film quality significantly.

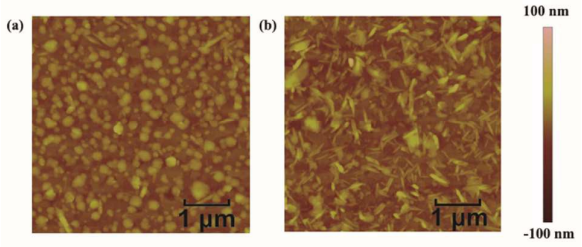

Figure 4 Tapping-mode AFM topography (5×5 μm) of spin-coated **AZOCP** (a) and **AZOCP-CSA** (b) films on ITO substrates, respectively.

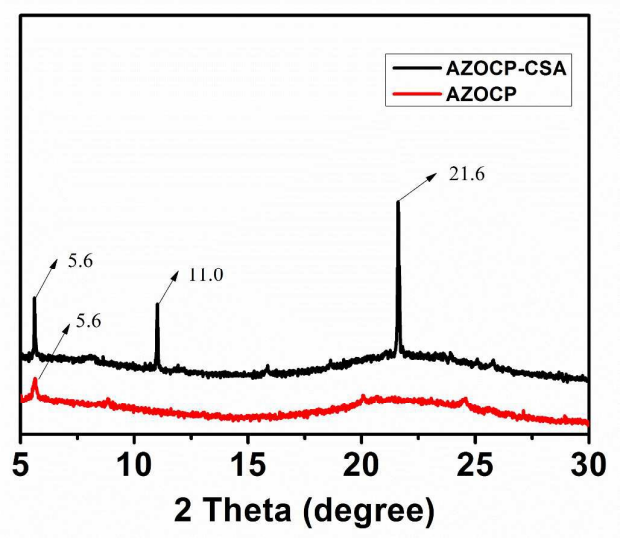

Figure 5 XRD patterns of **AZOCP** and **AZOCP-CSA** spin coated films onto quartz glass substrates.

In order to measure the crystalline order within the films, X-ray diffraction (XRD) experiments were performed on the spin-coated films. From the XRD patterns (Figure 5), **AZOCP** films showed an unconspicuous diffraction peak at 2θ = 5.6° of **AZOCP** corresponds to a d-spacing of ca. 15.8 Å. However, the ''counterpart'' compound **AZOCP-CSA** film was observed a higher intensity peak at 2θ = 5.6° and another strong peak at 2θ = 11° and 21.6° are corresponding to the d-spacing distances of15.8 Å, 8.0 Å and 4.1 Å, respectively. Furthermore, one diffraction angle of **AZOCP-CSA** is approximately two times larger than the other. These results indicate that the **AZOCP-CSA** molecule formed a highly ordered crystalline and a close layer-by-layer stacking structure in the thin film state that is favorable for forming highly efficient pathways for charge carrier transport and to obtain good memory performance. [42]

Current–voltage (I–V) characteristics of the memory devices

The memory effect of the **AZOCP** devices was explored first, and the current–voltage (I–V) characteristics are shown in Figure 6a. The fabricated Au/**AZOCP**/ITO memory devices have a resistance of about 5.9 K Ohm, and are in high resistance state (HRS) or OFF state. The arrows indicate thevoltage sweeping direction. Under a positively biased voltage sweeping, the current increases abruptly and reaches the compliance current (10^{-2} A) at around 2.5 V, indicating that the device has been switched from a HRS to a low resistance state (LRS or ON state) (sweep 1 of Figure 6a). This transition can be defined as the "Write" or "SET" process and the ON/OFF ratio of ~10^2 can be obtained. We defined ON/OFF ratio as RHRS/RLRS, where RHRS and RLRS are the resistance values in the HRS and LRS, respectively. The device remains at the ON state, even after the power is turned off or during the subsequent forward voltage sweeping (sweeps 2). Meanwhile, the current abruptly decreased during the sweep from 0 to -3 V, which is the transition

from LRS to HRS. This transition serves as the "Erase" or "RESET" process of a rewritable device. The OFF state can be maintained in the final sweep from -3 to 0 V (sweeps 4). Therefore, **AZOCP**-based device has potential applications for non-volatile data storage.

Compared with the Au/**AZOCP**/ITO devices, the Au/**AZOCP-CSA**/ITO devices exhibited much smoother I–V characteristics during the resistive-switching process. As shown in Figure 6d, the Au/**AZOCP-CSA**/ITO memory cells was in the HRS. When a positively biased potential sweep from 0 to 3 V was applied (sweep 1 in the Figure 6d), the current increased consecutively from ~10^{-6} A to ~10^{-2} A, indicating that the device had been set to the LRS by the positive forward sweep. This "Write" (or "SET") process was confirmed by the subsequent positive backward potential sweep from 3 to 0 V (sweep 2). In the following sweep from 0 to −3 V (sweep3), the device abruptly decreased to the HRS. The Au/**AZOCP-CSA**/ITO devices can remains at the HRS by applying a negatively-biased voltage sweeping from -3 V to 0 V (sweeps 4). The value of the ON/OFF ratio for **AZOCP-CSA**-base devices was 10^5. Compared with the Au/**AZOCP**/ITO device, the **AZOCP-CSA**-base device has higher ON/OFF ratio, which is helpful to avoid false programming and error readout problems.

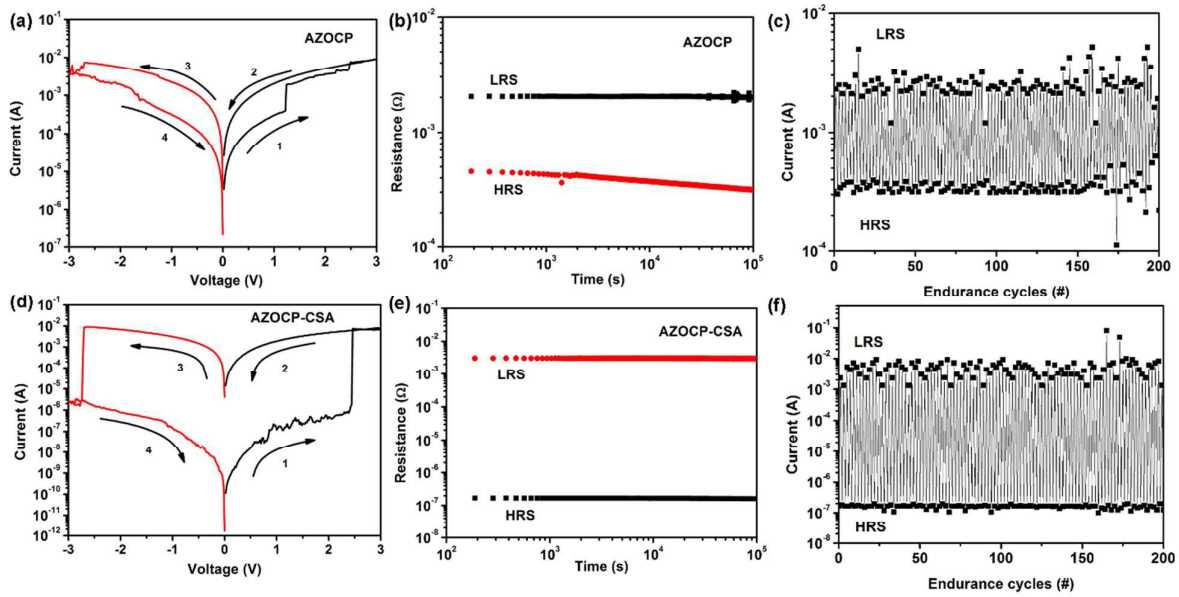

Figure 6 Current–voltage (I–V) characteristics of Au/**AZOCP**/ITO and Au/**AZOCP-CSA**/ITO memory device(a and d); the effect of retention time (b and e) and the endurance cycles of Au/**AZOCP**/ITO and Au/**AZOCP-CSA**/ITO memory device under a constant stress of -1.0 V (c and f).

The retention times of the RLRS and the RHRS of the Au/**AZOCP**/ITO and Au/**AZOCP-CSA**/ITO device are shown in Figure 6b and 6e. Under a constant stress of -1 V, **AZOCP-CSA**-based devices is observed more stability and no significant degradation in current for any of the states at least 10^5 s during the readout test. The endurance cycles of the Au/**AZOCP-CSA**/ITO device is much better than that of the Au/**AZOCP**/ITO device (as shown in Figure 6c and 6f). The rewritable cycles (write-read-erase-read) of **AZOCP-CSA**-base device could be repeated over 200 times and almost no attenuation.

Memory mechanism

First of all, we choose Au electrode instead of Al electrode in order to avoid the formation of Al_2O_x layer to affect the bistable memory performance.[43] Moreover, the low LRS current density (10^{-2} A) is lower than current compliance (10^{-1} A) and the lack of necessary forming process or device breakdown in our devices are speculated to exclude the metal filament mechanism.[44] To explain the current flow by adding an applied voltage, carrier transport mechanisms were analyzed through isothermal I–V correction. The related physical models have been described by follows: space-charge-limited conduction (SCLC; including ohmic conduction ($I \approx V$) and child's law region ($I \approx V^2$)). As shown in Figure 7, the I-V curve of LRS and HRS of Au/**AZOCP**/ITO devices satisfactorily fits the classical SCLC model. However, there are two different regions in the HRS of Au/**AZOCP-CSA**/ITO device. At the low voltage region of HRS, standard ohmic conduction model is dominated. It suggests a linear relationship of I–V curve ($I \propto V^{1.15}$), whereas in the high voltage region, the current density shows the square dependence of the voltage that confirms the child's mode ($I \propto V^{2.37}$) (Figure 7b). The SCLC can determine the charge carrier injection and hopping through the thin films in HRS. When the voltage continue to

increase and the current density increases exponentially to LRS. The charge injection/conduction in LRS (inset of Figure 7b) is well fitted to the SCLC model.

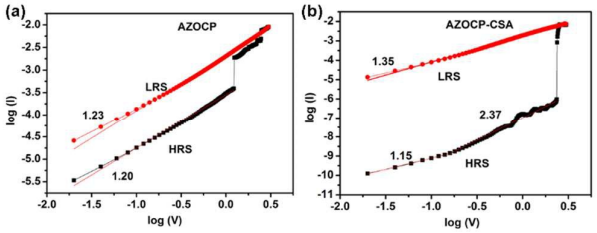

Figure 7 Experimental and fitted I–V curves of Au/**AZOCP**/ITO (a) and Au/**AZOCP-CSA**/ITO (b) memory device in both the ON and OFF states during the SET process.

To better understand the electronic process occurring inside the thin film. Theoretical calculations were performed using density-functional program DMol3.[45,46] The hybrid functional B3LYP,[47,48] together with a double numerical plus polarization (DNP) basis set, was employed. For simplification, the camphorsulfonic acid in **AZOCP-CSA** are omited in the computational models; this representation has little impact on the calculation results. The calculated results on HOMO, LUMO and energy gap (E_{gap}) are listed in Table S1. Compared the E_{gap} of **AZOCP** and **AZOCP-CSA**, the **AZOCP-CSA** has lower E_{gap}, which make charge carrier migration easier.

The molecular orbital (HOMO-2, HOMO-1, HOMO, LUMO, LUMO+1) and the electrostatic surface potential (ESP) of **AZOCP** and **AZOCP-CSA** molecules were plotted, and shown in Figure 8. The ESP plots of **AZOCP** and **AZOCP-CSA** molecules both show an open channel along the molecular backbone with continuous positive electrostatic potential, providing a path to allow charge carrier migration. For **AZOCP** molecule, electrons transit readily from HOMO orbital to LUMO orbital under external electric field, forming the locally excited state. Meanwhile, electrons in HOMO-2 can overcome the energy barrier between HOMO-2 and HOMO and fill the generated holes in HOMO, followed by the spontaneous electron transition from HOMO-1 to HOMO-2. As a result, a charge-transfer (CT) interaction can occur in **AZOCP** molecule between the electron donor moieties and the electron acceptor moieties. For **AZOCP-CSA** molecule, a similar charge transfer process is also formed. However, the salification enhances the electron-withdrawing ability of acceptor moiety, so the HOMO and LUMO orbitals of **AZOCP-CSA** molecules show more obvious separation in ground state, with HOMO mostly localizing on donor areas and LUMO mostly localizing on acceptor areas.

We speculated that the mechanism of the resistance-switching effects of the **AZOCP** and **AZOCP-CSA** devices could be the electric-field-induced charge transfer effect. Without external electric field, the electrons in **AZOCP** and **AZOCP-CSA** molecules were stable, and the as-fabricated device was in the HRS. When applied a positive bias, the charge transport pathways will form, and will switch the Au/**AZOCP** or **AZOCP-CSA**/ITO device from the HRS to the LRS. However, the salification can significantly enhance the electron-withdrawing ability of pyridine group,[49,50] resulting in a stronger intramolecular CT in **AZOCP-CSA**. There have been reported that changing the charge transfer ability of D-A molecules can tune memory effects.[51] So the better performance (larger ON/OFF ratio and more stable of each electric conductive state). of the **AZOCP-CSA**-based device could due to the stronger intramolecular CT effect. Application of a reverse positive bias to the **AZOCP**-based or **AZOCP-CSA**-based device can extract electrons from the acceptor moieties and program the device back to the HRS.[52] The nonvolatile nature of the LRS is due to the intensive electron delocalization in the acceptor moieties stabilized the conductive CT state.[53]

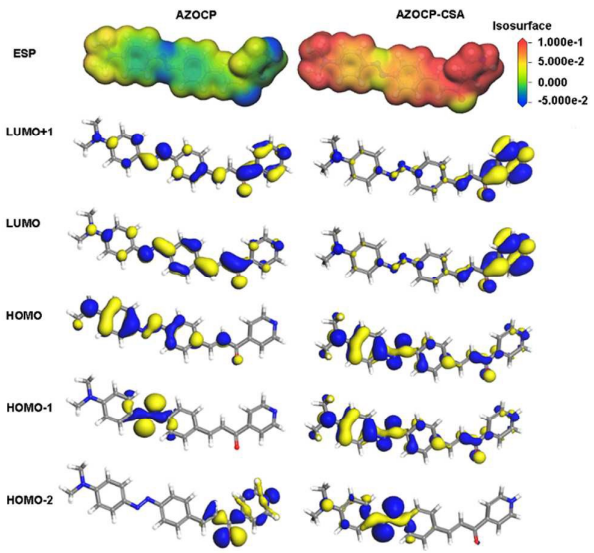

Figure 8 The HOMO-2, HOMO-1, HOMO, LUMO, LUMO+1 orbital and molecular ESP from DFT simulation result of **AZOCP** and **AZOCP-CSA.**

In order to further investigate the effect of salification on the device performance. We synthesized another new molecule with pyridine group: 3-(2-(dodecyloxy)-4-((4-nitrophenyl)diazenyl) phenyl)-1-(pyridin-4-yl)prop-2-en-1-one (**AZOCP2**) and its camphorsulfonic acid salification compound (**AZOCP2-CSA**) through the similar method mentioned above (as shown in Scheme S1). Further we studied the resistive memory properties of this compound based memories (as shown in Figure S6). After salification the compound **AZOCP2-CSA** was also shown a higher ON/OFF raito (from ~10^3 to ~10^4) and more stablable retention times (Figure S6). So we think that this kind of organic molecule with pyridine group system might improve the resistive memory properties by salification.

Conclusions

In summary, we designed and synthesised a new small molecule **AZOCP** and its salification compound **AZOCP-CSA**. From the UV-vis absorbance spectra, AFM and XRD measurement, the **AZOCP-CSA** molecule shows a stronger π–π conjugation and leads to a more ordered stacking nanocrystalline film. Moverover, the Au/**AZOCP-CSA**/ITO memory device has a higher ON/OFF raito and more stablable retention times and longer rewritable cycles than the Au/**AZOCP**/ITO memory device. The salification can promote the transport of charge carriers to promote memory performance in resistive switching. We demonstrate a very simple but effective strategy to improve organic resistive memory devices with good performance.

Acknowledgements

The authors thank the Chinese Natural Science Foundation (21336005, 21176164 and 21371128), Qing-Lan Project of Jiangsu Province and the Major Project of Department of Education in Jiangsu Province (15KJA150008).

References

1 Y. Chen, G. Liu, C. Wang, W. Zhang, R.-W. Li and L. Wang, *Mater. Horiz.*, 2014, **1**, 489-506.

2 X. Marti, I. Fina, C. Frontera, J. Liu, P. Wadley, Q. He, R. J. Paull, J. D. Clarkson, J. Kudrnovsky, I. Turek, J. Kunes, D. Yi, J. H. Chu, C. T. Nelson, L. You, E. Arenholz, S. Salahuddin, J. Fontcuberta, T. Jungwirth and R. Ramesh, *Nat. Mater.*, 2014, **13**, 367-374.

3 C. D. Wright, Y. Liu, K. I. Kohary, M. M. Aziz and R. J. Hicken, *Adv. Mater.*, 2011, **23**, 3408-3413.

4 J. J. Yang, F. Miao, M. D. Pickett, D. A. A. Ohlberg, D. R. Stewart, C. N. Lau and R. S. Williams, *Nanotechnology*, 2009, **20**, 215201-215209.

5 H. J. Koo, J. H. So, M. D. Dickey and O. D. Velev, *Adv. Mater.*, 2011, **23**, 3559-3564.

6 E. N. Oskoee and M. Sahimi, *Phys. Rev. E: Stat., Nonlinear, Soft Matter Phys.*, 2011, **83**, 031105-031108.

7 Q. D. Ling, D. J. Liaw, C. Zhu, D. S. H. Chan, E. T. Kang, K. G. Neoh, *Prog. Polym. Sci.* 2008, **33**, 917.

8 S. Song, B. Cho, T. W. Kim, Y. Ji, M. Jo, G. Wang, M. Choe, Y. H. Kahng, H. Hwang and T. Lee, Adv. Mater., 2010, **22**, 5048-5052.

9 B. B. Cui, J. H. Tang, J. Yao and Y. W. Zhong, *Angew. Chem. Int. Ed.*, 2015, **54**, 9192-9197.

10 C. T. Poon, D. Wu, W. H. Lam and V. W. Yam, *Angew. Chem. Int. Ed.*, 2015, **54**, 10569-10573.

11 S. E. Savel'ev, A. S. Alexandrov, A. M. Bratkovsky and R. S. Williams, *Nanotechnology*, 2011, **22**, 254011-254017.

12 X. Sun, G. Li, L. Ding, N. Yang and W. Zhang, *Appl. Phys. Lett.*, 2011, **99**, 072101-072103.

13 J. Fang, H. You, J. Chen, J. Lin and D. Ma, *Inorg. Chem.*, 2006, **45**, 3701-3704.

14 J. Xiao, Z. Yin, H. Li, Q. Zhang, F. Boey, H. Zhang and Q. Zhang, *J. Am. Chem. Soc.*, 2010, **132**, 6926-6928.

15 C. Simao, M. Mas-Torrent, J. Casado-Montenegro, F. Oton, J. Veciana and C. Rovira, *J. Am. Chem. Soc.*, 2011, **133**, 13256-13259.

16 B. Hu, C. Wang, J. Wang, J. Gao, K. Wang, J. Wu, Guodong Zhang, Wangqiao Cheng, B. Venkateswarlu, M. Wang, P. S. Leea and Q. Zhang, *Chem. Sci.*, 2014, **5**, 3404.

17 S. Miao, H. Li, Q. Xu, Y. Li, S. Ji, N. Li, L. Wang, J. Zheng and J. Lu, *Adv. Mater.*, 2012, **24**, 6210-6215.

18 P. Gu, J. He, G. Long, C. Wang, and W. Chen, Q. Xu, J. Lu and Q. Zhang, *J. Mater. Chem. C*, 2015, **3**, 3167--3172.

19 Y. Zhang, H. Zhuang, Y. Yang, X. Xu, Q. Bao, N. Li, H. Li, Q. Xu, J. Lu and L. Wang, *J. Phys. Chem. C*, 2012, **116**, 22832-22839.

20 Z. Liu, E. Shi, Y. Wan, N. Li, D. Chen, Q. Xu, H. Li, J. Lu, K. Zhang and L. Wang, *J. Mater. Chem. C*, 2015, **3**, 2033-2039.

21 Z. Liu, J. He, H. Zhuang, H. Li, N. Li, D. Chen, Q. Xu, J. Lu, K. Zhang and L. Wang, *J. Mater. Chem. C*, 2015, **3**, 9145-9153.

22 J. S. Lee, Y. M. Kim, J. H. Kwon, J. S. Sim, H. Shin, B. H. Sohn and Q. Jia, *Adv. Mater.*, 2011, **23**, 2064-2068.

23 S. J. Liu, P. Wang, Q. Zhao, H. Y. Yang, J. Wong, H. B. Sun, X. C. Dong, W. P. Lin and W. Huang, *Adv. Mater.*, 2012, **24**, 2901-2905.

24 C. Ye, Q. Peng, M. Li, J. Luo, Z. Tang, J. Pei, J. Chen, Z. Shuai, L. Jiang and Y. Song, *J. Am. Chem. Soc.*, 2012, **134**, 20053-20059.

25 C. Wang, B. Hu, J. Wang, J. Gao, G. Li, W.-W. Xiong, B. Zou, M. Suzuki, N. Aratani, H. Yamada, F. Huo, P. S. Lee and Q. Zhang, *Chem. - Asian J.*, 2015, **10**, 116-119.

26 G. Li, K. Zheng, C. Wang, K. S. Leck, F. Hu, X. W. Sun and Q. Zhang, *ACS Appl. Mater. Interfaces*, 2013, **5**, 6458.

27 P. Y. Gu, F. Zhou, J. Gao, G. Li, C. Wang, Q. F. Xu, Q. Zhang and J. M. Lu, *J. Am. Chem. Soc.*, 2013, **135**, 14086.

28 L. Xie, Q. Ling, X. Hou and W. Huang, *J. Am. Chem. Soc.*, 2008, **130**, 2120-2121.

29 S. K. Hwang, J. M. Lee, S. Kim, J. S. Park, H. I. Park, C. W. Ahn, K. J. Lee, T. Lee and S. O. Kim, *Nano Lett*, 2012, **12**, 2217-2221.

30 J. H. A. Smits, S. C. J. Meskers, R. J. Janssen, *Adv. Mater.* 2005,**17**, 1169-1173.

31 F. Verbakel, S. C. J. Meskers, R. J. Janssen, *Chem. Mater.* 2006**,18**, 2707-2712.

32 S. Miao, Y. Zhu, Q. Bao, H. Li, N. Li, S. Ji, Q. Xu,J. Lu, and L. Wang, *J. Phys. Chem. C,* 2014*,* **118***,* 2154−2160.

33 A. Tilborg, B. Norberg and J. Wouters, *Eur. J. Med. Chem.*, 2014, **74**, 411-426.

34 M. Wu, Z. W. Wang, Y. X. Liu, H. B. Song, A. Zhang, L. H. Meng and Q. M. Wang, *New J. Chem.*, 2013, **37**, 1817-1822.

35 B. Hu, X. Zhu, X. Chen, L. Pan, S. Peng, Y. Wu, J. Shang, G. Liu, Q. Yan and R. W. Li, *J. Am. Chem. Soc.*, 2012, **134**, 17408-17411.

36 J. Liu, J. W. Y. Lam and B. Z. Tang, *J. Inorg. Organomet. Polym.*, 2009, **19**, 249-285.

37 F. L. Ye, P. Y. Gu, F. Zhou, H. F. Liu, X. P. Xu, H. Li, Q. F. Xu and J. M. Lu, *Polymer*, 2013, **54**, 3324-3333.

38 H. Li, A. G. McDonald, *Ind. Crops Prod.*, 2014, **62**, 67-76.

39 H. Li, G. Sivasankarapillai, A. G. McDonald, *Ind. Crops Prod.*, 2015, **67**, 143-154.

40 S. Kim, T. K. An, J. Chen, I. Kang, S. H. Kang, D. S. Chung, C. E. Park, Y. H. Kim and S. K. Kwon, *Adv. Funct. Mater.*, 2011, **21**, 1616-1623.

41 F. C. Spano, *Acc. Chem. Res.*, 2010, **43**, 429-439.
42 L. Li, P. Gao, K. C. Schuermann, S. Ostendorp, W. Wang, C. Du, Y. Lei, H. Fuchs, L. Cola and L. Chi, *J. Am. Chem. Soc.*, 2010, **132**, 8807–8809.
43 A. D. Yu, T. Kurosawa, Y. H. Chou, K. Aoyag, T. Higashihara, M. Ueda, C. L. Liu, and W. C. Chen, *ACS Appl. Mater. Interfaces* 2013, **5**, 4921−4929.
44 F.Zhuge, B. Hu, C. He, X. Zhou, Z. Liu and R. W. Li, *Carbon,* 2011, **49**, 3796−3802.
45 B. Delley, *J. Chem. Phys.*, 1990, **92**, 508-517.
46 B. Delley, *J. Chem. Phys.*, 2000, **113**, 7756-7764.
47 A. D. Becke, *J. Chem. Phys.*, 1993, **98**, 5648-5652.
48 P. Stephens, F. Devlin, C. Chabalowski and M. J. Frisch, *J. Phys. Chem.*, 1994, **98**, 11623-11627.
49 S. Moller, C. Perlov, W. Jackson, C. Taussig and S. R. Forrest, *Nature* 2003, **426**, 166.
50 R. Sim, M. Y. Chan, A. S. W. Wong andP. S. Lee, *Org. Electron.* 2011, **12**, 185.
51 C. L. Liu , W. C. Chen , *Polym.Chem*. 2011 , **2** , 2169 .
52 B. Zhang, G. Liu, Y. Chen, L. J. Zeng, C. X. Zhu, K. G. Neoh, C. Wang and E. T. Kang, *Chem. Eur. J*, 2011, **17**, 13646-13652.
53 W. Zhang, C. Wang, G. Liu, X. Zhu, X. Chen, L. Pan, H. Tan, W. Xue, Z. Ji, J. Wang, Y. Chen and R. W. Li, *Chem. Commun.*, 2014, **50**, 11856-11858.